# Frequency and Voltage Control Schemes for Three-Phase Grid-Forming Inverters

**Yemi Ojo** * **Mohammed Benmiloud** * **Ioannis Lestas** *

* *Department of Engineering, University of Cambridge, Trumpington Street, Cambridge, UK. Email: {yo259, mb2287, icl20}@cam.ac.uk*

**Abstract:** Grid-forming inverters play an important role in supporting power systems with low rotational inertia. Their frequency and voltage control policies must guarantee a synchronised operation, accurate power sharing amongst inverters, and a good transient response. Simultaneously achieving the latter two requirements is in general a non-trivial problem and existing schemes in the literature often focus on one of these two aspects. In this paper, we propose a simple frequency controller that uses the inverter output current as feedback to adapt its frequency, and also propose controllers for the regulation of the DC and AC voltages. We show that the proposed control architectures achieve both power sharing without a communication link, and desirable passivity properties that can enhance the dynamic performance. Closed loop stability of the grid-forming inverter with a dynamic load is also proven and simulations on advanced models are carried out to validate the results.

*Keywords:* Microgrids, grid-forming inverters, grid-forming control, passivity.

## 1. INTRODUCTION

In the last decades, power systems have witnessed high penetration of renewable energy sources connected to the grid through power electronic converters. Compared to synchronous generators (SGs), inverters have low inertia and operate on a faster time scale. As a result, most inverter control strategies rely on stiff SG-based non-renewable conventional grids for their voltage and frequency regulation. These control strategies are referred to as *grid-following* control. Despite the fact that grid-following operation is easy to implement, autonomous (standalone) operation capability is key for standalone inverter-based microgrids. To make the latter autonomous and reliable, it is necessary to develop effective *grid-forming* frequency and voltage control schemes for grid-forming inverters.

Several control strategies have been developed for grid-forming inverters. *Virtual oscillator* control employs nonlinear limit cycle oscillators Aracil and Gordillo (2002). Although this concept has been theoretically investigated and validated, its complexity makes the implementation of frequency and voltage regulation schemes an involved problem Milano et al. (2018). The *matching control* Arghir et al. (2018) strategy involves augmenting the inverter dynamics with an internal oscillator that sets frequency via the tracking of a desired DC voltage. However, the regulation of the DC voltage to track its reference eliminates the direct relationship between power sharing and the droop coefficients. *Droop control* approaches enhance inverters with similar behaviour to SGs. The common form is the active power based frequency control Chandorkar et al. (1993). Although it offers accurate power sharing for interconnected inverters without communication links Chandorkar et al. (1993), it has nonlinearities associated with the active power relation that can affect dynamic performance.

Traditionally, the AC-side output voltages of inverters have been controlled by actuating the pulse-width modulation (PWM) blocks through the modulating signals generated by the cascaded inner (current) and outer (voltage) control loops Pogaku et al. (2007). These cascaded loops introduce phase lags/delays, and can give oscillatory responses for interconnected inverters Milano et al. (2018).

It is often desirable that grid-forming inverters have appropriate passivity properties. This allows to deduce closed-loop stability when the AC-side is connected to a passive load, and also contributes to the stability of interconnected inverters. This is therefore a property we aim to maintain in the inverter models under the various control schemes proposed throughout the paper. The contribution of the paper can be summarized as follows.

- We propose a frequency control scheme that takes the inverter output current direct coordinate as feedback to adapt its frequency. This scheme provides active power sharing without a communication link. At the same time it is shown that it allows for strict passivity of the inverter model in the local reference frame. Furthermore, it circumvents the nonlinearity in the feedback policy associated with active power based frequency droop control.
- We propose inverter DC and AC-side voltage control schemes that allow the passivity properties of the inverter to be maintained.
- We evaluate the transient performance of the frequency and voltage control schemes proposed via simulations on advanced inverter models .

Preliminary work on frequency control via the use of output current was considered in Ojo et al. (2019) where a small-signal analysis was presented. Here passivity properties are investigated and voltage control policies that preserve those are considered. The paper is structured as follows. Notation and definitions are given in section 2. The inverter model is presented in section 3. The frequency and DC voltage control schemes proposed are presented in section 4. The inverter AC-side output voltage controller is proposed in section 5. Section 6 presents numerical results, and section 7 concludes the paper.

⋆ This work was supported by ERC starting grant 679774.

## 2. NOTATION AND DEFINITIONS

Let $\mathbb{R}_{\geq 0} := \{x \in \mathbb{R} | x \geq 0\}$, $\mathbb{R}_{>0} := \{x \in \mathbb{R} | x > 0\}$, $\mathbb{N}^* := \mathbb{N} \setminus \{0\}$. Given $n, p \in \mathbb{N}^*$, we use $0_n$ ($1_n$) to denote the column vector of all zeros (ones), $\mathbf{I}_n$ the $n \times n$ identity matrix, $0_{n\times p}$ the $n \times p$ matrix of all zeros, $\mathbf{e} := [1\ 0]^\top$, and $\mathcal{J} := \left[\begin{smallmatrix} 0 & 1 \\ -1 & 0 \end{smallmatrix}\right]$. Let $x = \text{col}(x_1, \ldots, x_n) \in \mathbb{R}^n$ denote a column vector with entries $x_i \in \mathbb{R}$, and whenever clear from context we use the notation $x = \text{col}(x_i) \in \mathbb{R}^n$. The Euclidean norm of $x \in \mathbb{R}^n$ is denoted by $\|x\|$, i.e. $\|x\|^2 = x^\top x$.

*Definition 2.1.* (Symmetric AC three-phase signals). $x_{abc} : \mathbb{R}_{\geq 0} \to \mathbb{R}^3$ denotes a symmetric three-phase AC signal of the form $x_{abc}(t) = \text{col}(\hat{X}(t)\sin(\theta(t)), \hat{X}(t)\sin(\theta(t) - \frac{2\pi}{3}), \hat{X}(t)\sin(\theta(t) + \frac{2\pi}{3}))$, where $\theta(t)$ is the phase angle that satisfies

$$\dot{\theta}(t) = \omega(t) \tag{1}$$

and $\hat{X}(t)$, $\omega(t)$ are respectively the amplitude and frequency, which are in general time varying variables that take values in $\mathbb{R}_{>0}$. Note also that $1_3^\top x_{abc} = 0$.

The time argument $t$ will often be omitted in the presentation for convenience in the notation.

*Definition 2.2.* The Park transformation matrix for a given $\theta$ is given by

$$T(\theta) = \sqrt{\frac{2}{3}} \begin{bmatrix} \sin(\theta) & \sin(\theta - \frac{2\pi}{3}) & \sin(\theta + \frac{2\pi}{3}) \\ \cos(\theta) & \cos(\theta - \frac{2\pi}{3}) & \cos(\theta + \frac{2\pi}{3}) \\ \frac{1}{\sqrt{2}} & \frac{1}{\sqrt{2}} & \frac{1}{\sqrt{2}} \end{bmatrix} \tag{2}$$

*Definition 2.3.* (Local Direct-Quadrature Coordinates). The representation of a signal $x_{abc}$ (Definition 2.1) in its Local Direct-Quadrature Coordinates (denoted by $x_{dq0}$) is given by

$$x_{dq0}(t) = T(\theta(t))x_{abc}(t). \tag{3}$$

where $T(\theta(t))$ is as in (2) with $\theta(t)$ the angle of signal $x_{abc}(t)$ as in Definition 2.1. Note that $x_{abc}$ can be obtained from a given $x_{dq0}$ using (4).

$$x_{abc}(t) = T^{-1}(\theta(t))x_{dq0}(t) \tag{4}$$

*Remark 2.4.* Since $x_{abc}$ is three-phase symmetric (Definition 2.1), the third component of $x_{dq0}$ is zero. We use the notation $x_{dq}$ to refer to the first two components of the vector in (3).

*Passivity.* We will use within the paper the notions of passivity and strict passivity as defined in (Khalil, 2015, Definition 6.3). We also say that a system with state vector $x$ and input $u$ (Khalil, 2015, eqns (6.6), (6.7)) is (strictly) passive about an equilibrium $x^*, u^*$ if the corresponding definition in (Khalil, 2015, Definition 6.3) holds, but with $x, u$ replaced by the deviations $x - x^*$, $u - u^*$ respectively.

## 3. GRID-FORMING INVERTER MODEL

Fig. 1 shows the topology of a three-phase grid-forming inverter including the DC circuit, the switching block, and the AC circuit.

The DC circuit consists of a controllable current source with current $i_{dc}$ that is a signal that takes values in $\mathbb{R}_{>0}$, in parallel with a conductance $G_{dc} \in \mathbb{R}_{>0}$ and capacitor $C_{dc} \in \mathbb{R}_{>0}$. The switching block consists of semiconductor switches. The AC circuit is fitted with an $LCL$ filter, which is an arrangement of an inductance $L_f \in \mathbb{R}_{>0}$ with resistance $R_f \in \mathbb{R}_{>0}$, a shunt capacitance $C_f \in \mathbb{R}_{>0}$ with conductance $G_s \in \mathbb{R}_{>0}$, and an inductance $L_c \in \mathbb{R}_{>0}$ with resistance $R_c \in \mathbb{R}_{>0}$. The electrical components $G_{dc}$, $R_f$, $G_s$ and $R_c$ represent the dissipative part of the system.

In practice, the switching block is actuated via a PWM scheme which is controlled by a three-phase sinusoidal modulating signal $m$ which is the control input of the form described in Definition 2.1.

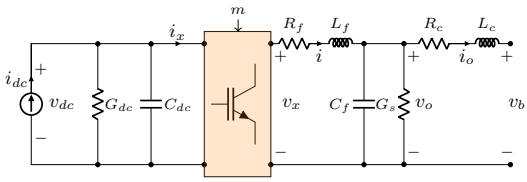


Fig. 1. Grid-forming inverter circuit diagram.

To present the physical model of the inverter, the following assumptions are made.

*Assumption 3.1.*

- The switching frequency of the PWM is assumed to be much higher than the natural frequencies of the power stage.
- The power generated on the DC-side is transferred to the AC-side without switching losses.

From the assumptions above the following relationships can be used $i_x = \frac{1}{2}m^\top i$ and $v_x = \frac{1}{2}mv_{dc}$. These then lead to the average model of the inverter in Fig. 1, which is a model commonly used in the literature and is given by:

$$\begin{aligned} C_{dc}\dot{v}_{dc} &= -G_{dc}v_{dc} + i_{dc} - \frac{1}{2}m^\top i \\ L_f\dot{i} &= -R_f i + \frac{1}{2}mv_{dc} - v_o \\ C_f\dot{v}_o &= -G_s v_o + i - i_o \\ L_c\dot{i}_o &= -R_c i_o + v_o - v_b \end{aligned} \tag{5}$$

where signal $v_{dc}$ takes values in $\mathbb{R}_{>0}$ and denotes the capacitor DC voltage, $i$, $i_o$, $v_o$, $v_b$ are signals that take values in $\mathbb{R}^3$ and denote the inverter input and output AC currents and voltages respectively. The modulating signal (control input) $m$ in the average model is a sinusoidal signal of the form described in Definition 2.1, hence it is commonly assumed in the literature (e.g. Pogaku et al. (2007)) that the inverter voltages and currents $i$, $i_o$, $v_o$, $v_b$ belong to the class of signals presented in Definition 2.1.

Considering the inverter local frequency $\omega$, and applying the $dq$ transformation (3) to system (5), the inverter model in local $dq$ coordinates is given by:

$$C_{dc}\dot{v}_{dc} = -G_{dc}v_{dc} + i_{dc} - \frac{1}{2}m_{dq}^\top i_{dq} \tag{6a}$$

$$L_f\dot{i}_{dq} = -R_f i_{dq} + \omega L_f \mathcal{J} i_{dq} + \frac{1}{2}m_{dq}v_{dc} - v_{odq} \tag{6b}$$

$$C_f\dot{v}_{odq} = -G_s v_{odq} + \omega C_f \mathcal{J} v_{odq} + i_{dq} - i_{odq} \tag{6c}$$

$$L_c\dot{i}_{odq} = -R_c i_{odq} + \omega L_c \mathcal{J} i_{odq} + v_{odq} - v_{bdq} \tag{6d}$$

where signals $i_{dq} = [i_d\ \ i_q]^\top$, $i_{odq} = [i_{od}\ \ i_{oq}]^\top$, $v_{dq} = [v_d\ \ v_q]^\top$, $v_{odq} = [v_{od}\ \ v_{oq}]^\top$, $v_{bdq} = [v_{bd}\ \ v_{bq}]^\top$ take values in $\mathbb{R}^2$ and denote the inverter $dq$ currents and voltages. The variable $m_{dq}$ denotes the $dq$ coordinates of the control input variable $m$. It takes values in $\mathbb{R}^2$ where $m_{dq} = [m_d\ \ m_q]^\top$.

Note that (6) involves the frequency $\omega$ and does not directly involve the angle $\theta$ of the signals in their $abc$ representation. The sinusoidal steady-state solution of (5) with associated steady-state frequency $\omega^*$ is mapped by the $dq$ transform to an equilibrium of (6). The steady-state solution of (6) can be obtained by setting its left-

hand side to zero. We complete the DC side with a DC current source proportional to the DC voltage as follows:

$$i_{dc} = i_{dc,ref} - \Lambda_P(v_{dc} - v_{dc,ref}) \tag{7}$$

where $i_{dc,ref}$, $v_{dc,ref}$, $\Lambda_P \in \mathbb{R}_{>0}$ are the DC current and voltage set-points, and proportional gain respectively.

The design of the frequency and voltage control schemes is based on the dq representation in (6) with $m_{dq}$ as the control input. Note that the three-phase control input $m$ in (5) (i.e. its *abc* representation) is given by [1]:

$$m(t) = T^{-1}(\theta(t))m_{dq0}(t) \tag{8}$$

where $\theta(t)$ satisfies $\omega(t) = \dot{\theta}(t)$, with the frequency $\omega(t)$ determined from a frequency control policy (described in section 4). The control signal $m_{dq}$ is determined by a voltage control policy (described in section 5). Due to the simpler representation of the system dynamics in dq coordinates in (6), the latter will be used for the analysis in the remainder of the paper.

The remaining part of the paper is organised as follows. We propose the frequency control scheme in section 4. Its active power sharing property is discussed in section 4.1. We show that it provides passivity properties in the local *dq* frame in section 4.2, and closed-loop stability when connected to a load (section 4.3). Furthermore, DC and AC-side voltage control policies that maintain the passivity properties provided by the proposed frequency control scheme are presented in sections 4.4 and 5 respectively.

We note that for the passivity property to lead to stability guarantees in general network topologies without simplifying assumptions on the line dynamics, the passivity property needs to be established in the common reference frame (see Watson et al. (2019)), and this will be investigated as part of future work. In this paper we demonstrate via simulations carried out on advanced models in section 6 that the interconnection of grid-forming inverters which implement the control policies presented gives good performance that is robust to load variations.

## 4. PROPOSED FREQUENCY CONTROL

For a secure and reliable interconnection, grid forming inverters must operate in a synchronised manner and achieve accurate active power sharing. It is desirable that the frequency controller of each inverter meets these control objectives with only local measurements to avoid communication requirements.

In the recently proposed *matching control* scheme Arghir et al. (2018), frequency is controlled via the DC voltage by means of proportional control. However, the regulation of the DC voltage to its reference eliminates the direct relationship between power sharing and the droop coefficients. Another scheme is the conventional active power based frequency droop control proposed in Chandorkar et al. (1993). Although it offers active power sharing without communication, nonlinearity is introduced in the feedback policy via the active power relation.

To remedy this issue, we propose a frequency controller that takes the inverter output current direct coordinate $i_{od} := \mathbf{e}^\top i_{odq}$ (i.e., the first component of $i_{odq}$) as feedback to adapt the frequency $\omega$ as follows:

$$\omega = \omega_n - k_p\, \mathbf{e}^\top i_{odq} \tag{9}$$

where $\omega_n$, $k_p \in \mathbb{R}_{>0}$ are the nominal frequency and droop gain respectively. As it will be discussed, the scheme (9) has the advantage of providing accurate active power sharing at steady state for interconnected grid-forming inverters without requiring communication (sections 4.1, 6). Moreover, it will be shown that this control scheme allows to have appropriate passivity properties for the inverter model (6)–(7) with less restrictive conditions relative to existing schemes in the literature (section 4.2). Furthermore, it will be shown that these passivity properties are maintained when an appropriate voltage control policy is also incorporated (sections 4.4, 5).

### *4.1 Active Power Sharing*

Consider a network of $N$ connected inverters. We say inverter $i$ is connected to inverter $j$ if their AC output terminals (i.e. the terminals with voltage difference $v_b$ in Fig. 1) are connected via a transmission line (an example of interconnection of two inverters is shown in Fig. 2). We say the inverters are synchronised if their frequencies are identical. In Proposition 4.1, we describe the power sharing achieved among synchronised inverters under the proposed frequency control policy (9) if synchronisation is achieved at equilibrium. To facilitate the readability of the manuscript, the AC voltage control policy is not presented at this stage. Nevertheless, it should be noted that Proposition 4.1 also holds if the AC voltage control policies (section 5) are implemented.

*Proposition 4.1.* (Power sharing). Consider a network of $N$ interconnected inverters where each inverter is described by (6)–(7). If an equilibrium point is reached where the inverters synchronise, the real powers $P_i^*$, $i = 1, \ldots, N$ of the inverters at the equilibrium point satisfy

$$\frac{P_i^*}{P_j^*} = \frac{\mathbf{e}^\top v_{odq,i}^*}{\mathbf{e}^\top v_{odq,j}^*}\, \frac{k_{p,j}}{k_{p,i}} \tag{10}$$

where $v_{odq,i}^*$, $v_{odq,j}^*$ are the equilibrium values of the inverter voltages $v_{odq,i}$, $v_{odq,j}$ respectively. Moreover, $P_i^* = P_j^*$ if $v_{odq,i}^* = v_{odq,j}^*$, and the droop gains satisfy $k_{p,i} = k_{p,j}$.

**Proof.** Given that synchronisation holds we have that $\omega_i^* = \omega_j^*$ for all inverters $i, j$. This implies $\omega_n - k_{p,i}\mathbf{e}^\top i_{odq,i}^* = \omega_n - k_{p,j}\mathbf{e}^\top i_{odq,j}^*$, where $i_{odq,j}^*$ is the equilibrium value of the current $i_{odq,j}$. This yields

$$\frac{\mathbf{e}^\top i_{odq,i}^*}{\mathbf{e}^\top i_{odq,j}^*} = \frac{k_{p,j}}{k_{p,i}} \tag{11}$$

Given the active power relation $P = (\mathbf{e}^\top v_{odq})(\mathbf{e}^\top i_{odq})$, the active powers of inverters $i$ and $j$ at the equilibrium point are given by $P_i^* = (\mathbf{e}^\top v_{odq,i}^*)(\mathbf{e}^\top i_{odq,i}^*)$, $P_j^* = (\mathbf{e}^\top v_{odq,j}^*)(\mathbf{e}^\top i_{odq,j}^*)$, respectively. We therefore get

$$\frac{P_i^*}{P_j^*} = \frac{\mathbf{e}^\top v_{odq,i}^*}{\mathbf{e}^\top v_{odq,j}^*}\, \frac{\mathbf{e}^\top i_{odq,i}^*}{\mathbf{e}^\top i_{odq,j}^*}$$

and using (11) we deduce the active power sharing relation (10). If $\mathbf{e}^\top v_{odq,i}^* = \mathbf{e}^\top v_{odq,j}^*$, and choose $k_{p,i} = k_{p,j}$, then $P_i^* = P_j^*$ trivially holds at steady state.

*Remark 4.2.* The relation (10) shows that the active power is shared among interconnected inverters according to the ratio $\frac{k_{p,j}}{k_{p,i}}$ since the voltages do not vary much in practice. If $k_{p,i} = k_{p,j}$ is chosen, equal active power is shared between the $i$th and $j$th inverters. See also section 6 where simulations on advanced model are carried out and the power sharing property is verified.

[1] Note that the third component of $m_{dq0}$ is always zero as noted in Remark 2.4.

### 4.2 Passivity

In this section we show that the proposed frequency controller (9) allows the inverter to satisfy a strict passivity property. The passivity property is established in the local $dq$ reference frame with respect to an equilibrium point $(x^*, u^*)$.

*Theorem 4.3.* (Strict Passivity in $dq$ Coordinates). Consider the grid-forming inverter model (6)–(7) with a constant modulating signal $m_{dq}$, together with control policy (9). Assume that for a given input $u^* = -v^*_{bdq}$ there exists an equilibrium $x^* = (v^*_{dc}, i^*_{dq}, v^*_{odq}, i^*_{odq})$ such that

$$C_f^2\|v^*_{odq}\|^2 + L_f^2\|i^*_{dq}\|^2 + \frac{L_c^2}{R_c^2}(i^*_{od})^2 - \frac{4L_c}{k_p}i^*_{oq} - \frac{4R_c}{k_p^2} < 0 \quad (12)$$

Then, the system with input $u = -v_{bdq}$ and output $y = i_{odq}$ described by (6), (7), (9) is strictly passive about the equilibrium point $(x^*, u^*)$.

**Proof.** Our proof is inspired by Arghir et al. (2018). Starting from the assumptions of the theorem, we define the error signals: $\tilde{v}_{dc} = v_{dc} - v^*_{dc}$, $\tilde{i}_{dq} = i_{dq} - i^*_{dq}$, $\tilde{v}_{odq} = v_{odq} - v^*_{odq}$, $\tilde{i}_{odq} = i_{odq} - i^*_{odq}$, $\tilde{v}_{bdq} = v_{bdq} - v^*_{bdq}$, $\tilde{\omega} = \omega - \omega^*$. For some $\omega^*$ the error coordinate model of (6)-(7) is given by

$$\begin{aligned}
C_{dc}\dot{\tilde{v}}_{dc} =& -(G_{dc} + \Lambda_P)\tilde{v}_{dc} - \frac{1}{2}m_{dq}^\top \tilde{i}_{dq} \\
L_f\dot{\tilde{i}}_{dq} =& -(R_f\mathbf{I}_2 - \omega^* L_f\mathcal{J} - \tilde{\omega}L_f\mathcal{J})\tilde{i}_{dq} + \tilde{\omega}L_f\mathcal{J}i^*_{dq} \\
&+ \frac{1}{2}m_{dq}\tilde{v}_{dc} - \tilde{v}_{odq} \\
C_f\dot{\tilde{v}}_{odq} =& -(G_s\mathbf{I}_2 - \omega^* C_f\mathcal{J} - \tilde{\omega}C_f\mathcal{J})\tilde{v}_{odq} \\
&+ \tilde{\omega}C_f\mathcal{J}v^*_{odq} + \tilde{i}_{dq} - \tilde{i}_{odq} \\
L_c\dot{\tilde{i}}_{odq} =& -(R_c\mathbf{I}_2 - \omega^* L_c\mathcal{J} - \tilde{\omega}L_c\mathcal{J})\tilde{i}_{odq} \\
&+ \tilde{\omega}L_c\mathcal{J}i^*_{odq} + \tilde{v}_{odq} - \tilde{v}_{bdq}
\end{aligned} \quad (13)$$

Consider the storage function $\mathcal{H}_1 : \mathbb{R}^7 \to \mathbb{R}_{>0}$ given by

$$\mathcal{H}_1 = \frac{1}{2}C_{dc}\tilde{v}_{dc}^2 + \frac{1}{2}\tilde{i}_{dq}^\top L_f\tilde{i}_{dq} + \frac{1}{2}\tilde{v}_{odq}^\top C_f\tilde{v}_{odq} + \frac{1}{2}\tilde{i}_{odq}^\top L_c\tilde{i}_{odq}. \quad (14)$$

The derivative of $\mathcal{H}_1$ along the trajectories of (13) is

$$\begin{aligned}
\dot{\mathcal{H}}_1 =& -\tilde{v}_{dc}^\top(G_{dc} + \Lambda_{dc})\tilde{v}_{dc} - \tilde{i}_{dq}^\top R_f\tilde{i}_{dq} - \tilde{v}_{odq}^\top G_s\tilde{v}_{odq} - \tilde{i}_{odq}^\top R_c\tilde{i}_{odq} \\
&- \tilde{i}_{odq_i}^\top\tilde{v}_{bdq_i} + \tilde{i}_{dc}\tilde{v}_{dc} + \frac{1}{2}\tilde{\omega}^\top L_f i^{*\top}_{dq}\mathcal{J}^\top\tilde{i}_{dq} + \frac{1}{2}L_f\tilde{i}_{dq}^\top\mathcal{J}i^*_{dq}\tilde{\omega} \\
&+ \frac{1}{2}\tilde{\omega}^\top C_f v^{*\top}_{odq}\mathcal{J}^\top\tilde{v}_{doq} + \frac{1}{2}C_f\tilde{v}_{odq}^\top\mathcal{J}v^*_{odq}\tilde{\omega} + \frac{1}{2}\tilde{\omega}^\top L_c i^{*\top}_{odq}\mathcal{J}^\top\tilde{i}_{odq} \\
&+ \frac{1}{2}L_c\tilde{i}_{odq}^\top\mathcal{J}i^*_{odq}\tilde{\omega}.
\end{aligned} \quad (15)$$

By our proposed frequency control scheme (9), the frequency error signal is obtained as $\tilde{\omega} = -k_p\mathbf{e}^\top\tilde{i}_{odq}$. Substituting this for $\tilde{\omega}$ in (15) gives the compact representation

$$\begin{aligned}
\dot{\mathcal{H}}_1 =& -\begin{bmatrix}\tilde{v}_{dc} & \tilde{i}_{dq}^\top & \tilde{v}_{odq}^\top & \tilde{i}_{odq}^\top\end{bmatrix}\mathcal{M}_1\begin{bmatrix}\tilde{v}_{dc} & \tilde{i}_{dq}^\top & \tilde{v}_{odq}^\top & \tilde{i}_{odq}^\top\end{bmatrix}^\top \\
&- \tilde{i}_{odq}^\top\tilde{v}_{bdq}
\end{aligned}$$

where the symmetric matrix $\mathcal{M}_1 \in \mathbb{R}^{7\times 7}$ is obtained as

$$\mathcal{M}_1 = \begin{bmatrix}(G_{dc} + \Lambda_P) & 0_{1\times 2} & 0_{1\times 2} & 0_{1\times 2} \\ 0_2 & R_f\mathbf{I}_2 & 0_{2\times 2} & p_1 \\ 0_2 & 0_{2\times 2} & G_s\mathbf{I}_2 & p_2 \\ 0_2 & p_1^\top & p_2^\top & p_3\end{bmatrix}, \quad (16)$$

$p_1 = \frac{1}{2}(L_f k_p\mathcal{J}i^*_{dq}\mathbf{e}^\top)$, $p_2 = \frac{1}{2}(C_f k_p\mathcal{J}v^*_{odq}\mathbf{e}^\top)$, $p_3 = R_{ci}\mathbf{I}_2 + \frac{1}{2}L_c k_p\left[\mathcal{J}i^*_{odq}\mathbf{e}^\top + (\mathcal{J}i^*_{odq}\mathbf{e}^\top)^\top\right]$. Evaluating all the leading principal minors of $\mathcal{M}_1$ shows that under condition (12), $\mathcal{M}_1$ is positive definite. Therefore, system (13) is strictly passive with input $-\tilde{v}_{bdq}$ and output $\tilde{i}_{odq}$.

*Remark 4.4.* Other schemes have been proposed in the literature that achieve passivity properties, such as the matching control Arghir et al. (2018). One of the advantages of the proposed frequency controller (9) is the fact that condition (12) does not depend on the DC-side gains, thus avoiding requirements for high gains that can be restrictive in practical implementations. The $k_p$ can be chosen sufficiently small to satisfy (12). Condition (12) provides also insight on choosing $R_c, L_c, C_f$ to complement the choice of $k_p$ and preserve the inverter passivity properties at the desired operating points.

*Remark 4.5.* The passivity property also allows to deduce global asymptotic stability when the inverter is connected to a constant impedance load. This will be discussed in section 4.3.

### 4.3 Closed-Loop Stability

By making use of the passivity properties of (6), (7), (9) discussed in section 4.2, we analyse the closed-loop stability of the grid-forming inverter when its AC-side is connected to a load. In this analysis, we consider a constant impedance dynamic load described by the following model

$$L_\ell\dot{i}_o = -R_\ell i_o + v_b \quad (17)$$

where $R_\ell, L_\ell \in \mathbb{R}_{>0}$ are the load resistance and inductance respectively. Applying the Park transformation (3) to the load model (17) yields

$$L_\ell\dot{i}_{odq} = -R_\ell i_{odq} + \omega L_\ell\mathcal{J}i_{odq} + v_{bdq}. \quad (18)$$

Corollary 4.6 is associated with the closed loop stability of the grid-forming inverter when connected to this load.

*Corollary 4.6.* (Closed-Loop Stability). Consider the grid-forming inverter model (6)-(7) with a constant modulating signal $m_{dq}$, together with control policy (9) and the dynamic load (18). Assume there exists an equilibrium point $x^* = (v^*_{dc}, i^*_{dq}, v^*_{odq}, i^*_{odq})$ such that

$$C_f^2\|v^*_{odq}\|^2 + L_f^2\|i^*_{dq}\|^2 + \frac{\bar{L}_c^2}{\bar{R}_c^2}(i^*_{od})^2 - \frac{4\bar{L}_c}{k_p}i^*_{oq} - \frac{4\bar{R}_c}{k_p^2} < 0 \quad (19)$$

where $\bar{L}_c = L_c + L_\ell, \bar{R}_c = R_c + R_\ell$. Then, the equilibrium point $x^*$ is unique and globally asymptotically stable.

**Proof.** The proof follows that of Theorem 4.3. We adopt the notation used in the proof of Theorem 4.3 where the superscript $\tilde{\cdot}$ is used to denote the deviation of a signal from its equilibrium value. The error dynamics of the load (18) about the equilibrium point $(i^*_{odq}, v^*_{bdq})$ is:

$$L_\ell\dot{\tilde{i}}_{odq} = -(R_\ell\mathbf{I}_2 - \omega^* L_\ell\mathcal{J} - \tilde{\omega}L_\ell\mathcal{J})\tilde{i}_{odq} + \tilde{\omega}\mathcal{J}i^*_{odq} + \tilde{v}_{bdq}. \quad (20)$$

Consider the Lyapunov function $\mathcal{H}_2 : \mathbb{R}^7 \to \mathbb{R}_{>0}$ given by

$$\mathcal{H}_2 = \mathcal{H}_1 + \frac{1}{2}\tilde{i}_{odq}^\top L_\ell\tilde{i}_{odq} \quad (21)$$

where $\mathcal{H}_1$ is as defined in (14). The derivative of $\mathcal{H}_2$ along the trajectories of (13), (20) is

$$\dot{\mathcal{H}}_2 = -\begin{bmatrix}\tilde{v}_{dc} & \tilde{i}_{dq}^\top & \tilde{v}_{odq}^\top & \tilde{i}_{odq}^\top\end{bmatrix}\mathcal{M}_2\begin{bmatrix}\tilde{v}_{dc} & \tilde{i}_{dq}^\top & \tilde{v}_{odq}^\top & \tilde{i}_{odq}^\top\end{bmatrix}^\top \quad (22)$$

where the symmetric matrix $\mathcal{M}_2 \in \mathbb{R}^{7\times 7}$ is given by

$$\mathcal{M}_2 = \begin{bmatrix}(G_{dc} + \Lambda_P) & 0_{1\times 2} & 0_{1\times 2} & 0_{1\times 2} \\ 0_2 & R_f\mathbf{I}_2 & 0_{2\times 2} & p_1 \\ 0_2 & 0_{2\times 2} & G_s\mathbf{I}_2 & p_2 \\ 0_2 & p_1^\top & p_2^\top & p_4\end{bmatrix}, \quad (23)$$

$p_1 = \frac{1}{2}(L_f k_p\mathcal{J}i^*_{dq}\mathbf{e}^\top)$, $p_2 = \frac{1}{2}(C_f k_p\mathcal{J}v^*_{odq}\mathbf{e}^\top)$, $p_4 = (R_c + R_\ell)\mathbf{I}_2 + \frac{1}{2}(L_c + L_\ell)k_p\left[\mathcal{J}i^*_{odq}\mathbf{e}^\top + (\mathcal{J}i^*_{odq}\mathbf{e}^\top)^\top\right]$. By

evaluating all the leading principal minors of $\mathcal{M}_2$ we see that under condition (19), $\mathcal{M}_2$ is positive definite. Hence, the steady state $x^*$ is asymptotically stable by Lyapunov's direct method. The radial unboundedness of $\mathcal{H}_2$ guarantees global asymptotic stability.

*Remark 4.7.* The strict passivity property stated in Theorem 4.3 is essential for Corollary 4.6 as (12) is necessary for (19) to be satisfied.

### *4.4 DC Voltage Regulation*

As (7) may not regulate the DC-bus voltage $v_{dc}$ to the desired set-point $v_{dc,ref}$, we propose a DC voltage proportional-integral (PI) controller that achieves this. It is shown in this section that this controller preserves the passivity properties established in section 4.2, and therefore closed-loop stability is guaranteed when the inverter AC-side is connected to a load of the form (18). The DC voltage PI controller is given by

$$i_{dc} = i_{dc,ref} - \Lambda_P(v_{dc} - v_{dc,ref}) - \Lambda_I \int_0^t (v_{dc} - v_{dc,ref})\, d\tau \quad (24)$$

where $i_{dc,ref}$, $\Lambda_P, \Lambda_I \in \mathbb{R}_{>0}$ are the constant associated with the DC-side current, the proportional and integral gains respectively.

The closed loop system is given by (6), (9) augmented with (24). The integral term introduces an additional state, denoted by $\zeta$, and its steady state value is denoted by $\zeta^*$. We will also use the superscript $\tilde{}$ to denote the deviation of a variable from its equilibrium value, i.e. $\tilde{\zeta} = \zeta - \zeta^*$. Considering deviations from an equilibrium point $(v_{dc}^*, i_{dq}^*, v_{odq}^*, i_{odq}^*, \zeta^*)$ the error coordinate model is

$$\begin{aligned}
\dot{\tilde{\zeta}} &= \tilde{v}_{dc} \\
C_{dc}\dot{\tilde{v}}_{dc} &= -(G_{dc_i} + \Lambda_P)\tilde{v}_{dc} - \Lambda_I\tilde{\zeta} - \frac{1}{2}m_{dq}^\top \tilde{i}_{dq} \\
L_f\dot{\tilde{i}}_{dq} &= -(R_f\mathbf{I}_2 - \omega^* L_f\mathcal{J} + k_p\mathbf{e}^\top\tilde{i}_{odq}L_f\mathcal{J})\tilde{i}_{dq} \\
&\quad - k_p\mathbf{e}^\top\tilde{i}_{odq}L_f\mathcal{J}i_{dq}^* + \frac{1}{2}m_{dq}\tilde{v}_{dc} - \tilde{v}_{odq} \\
C_f\dot{\tilde{v}}_{odq} &= -(G_s\mathbf{I}_2 - \omega^* C_f\mathcal{J} + k_p\mathbf{e}^\top\tilde{i}_{odq}C_f\mathcal{J})\tilde{v}_{odq} \\
&\quad - k_p\mathbf{e}^\top\tilde{i}_{odq}C_f\mathcal{J}v_{odq}^* + \tilde{i}_{dq} - \tilde{i}_{odq} \\
L_c\dot{\tilde{i}}_{odq} &= -(R_c\mathbf{I}_2 - \omega^* L_c\mathcal{J} + k_p\mathbf{e}^\top\tilde{i}_{odq}L_c\mathcal{J})\tilde{i}_{odq} \\
&\quad - k_p\mathbf{e}^\top\tilde{i}_{odq}L_c\mathcal{J}i_{odq}^* + \tilde{v}_{odq} - \tilde{v}_{bdq}
\end{aligned} \quad (25)$$

*Theorem 4.8.* (DC Voltage Regulation). Consider the grid forming inverter model (25) with a constant modulating signal $m_{dq}$, and assume that (12) is satisfied. Then the system with input $u = -\tilde{v}_{bdq}$ and output $y = \tilde{i}_{odq}$ described by (25) is passive. Moreover, suppose the load (18) is present (with error dynamics given by (20)) with condition (19) satisfied. Then the equilibrium point of (25), (20) is globally asymptotically stable.

**Proof.** Consider the storage function $\mathcal{H}_3 : \mathbb{R}^8 \to \mathbb{R}_{>0}$ given by:

$$\mathcal{H}_3 = \mathcal{H}_1 + \frac{1}{2}\Lambda_I\tilde{\zeta}^2 \quad (26)$$

where $\mathcal{H}_1$ is as defined in (14). Its time derivative along the trajectories of system (25) is

$$\begin{aligned}
\dot{\mathcal{H}}_3 = &- \begin{bmatrix}\tilde{v}_{dc} & \tilde{i}_{dq}^\top & \tilde{v}_{odq}^\top & \tilde{i}_{odq}^\top\end{bmatrix}\mathcal{M}_1\begin{bmatrix}\tilde{v}_{dc} & \tilde{i}_{dq}^\top & \tilde{v}_{odq}^\top & \tilde{i}_{odq}^\top\end{bmatrix}^\top \\
&- \tilde{i}_{odq}^\top\tilde{v}_{bdq}
\end{aligned}$$

where the symmetric matrix $\mathcal{M}_1 \in \mathbb{R}^{7\times 7}$ is as in (16). With (12) satisfied, $\mathcal{M}_1$ is positive definite and (25) with input $-\tilde{v}_{bdq}$ and output $\tilde{i}_{odq}$ is passive.

Suppose the AC-side is connected to the load (18). We use LaSalle's theorem to prove global asymptotic stability of the equilibrium point. Consider the Lyapunov-like function $\mathcal{H}_4 : \mathbb{R}^8 \to \mathbb{R}_{>0}$ given by

$$\mathcal{H}_4 = \mathcal{H}_2 + \frac{1}{2}\Lambda_I\tilde{\zeta}^2 \quad (27)$$

where $\mathcal{H}_2$ is as defined in (21). Its time derivative along the trajectories of (20), (25) is obtained as

$$\dot{\mathcal{H}}_4 = - \begin{bmatrix}\tilde{v}_{dc} & \tilde{i}_{dq}^\top & \tilde{v}_{odq}^\top & \tilde{i}_{odq}^\top\end{bmatrix}\mathcal{M}_2\begin{bmatrix}\tilde{v}_{dc} & \tilde{i}_{dq}^\top & \tilde{v}_{odq}^\top & \tilde{i}_{odq}^\top\end{bmatrix}^\top$$

where the symmetric matrix $\mathcal{M}_2 \in \mathbb{R}^{7\times 7}$ is as defined in (23). If (19) is satisfied, $\mathcal{M}_2$ is positive definite which implies that $\dot{\mathcal{H}}_4 \leq 0$. Since $H_4$ is also radially unbounded its level sets form compact invariant sets that can be chosen arbitrarily large. From the fact that $\mathcal{M}_2$ is positive definite, $\dot{\mathcal{H}}_4 = 0$ implies that all the states of closed-loop system (20), (25) excluding $\tilde{\zeta}$ are equal to zero. Bearing this in mind and from (25), the only invariant set for which $\dot{\mathcal{H}}_4 = 0$ is the origin (i.e. $\tilde{\zeta}$ is also equal to zero). Hence, it follows from LaSalle's theorem that the equilibrium point of the closed-loop system (20), (25) is globally asymptotically stable.

## 5. AC OUTPUT VOLTAGE REGULATION

We have thus far considered a constant modulating signal $m_{dq}$. However, this may not guarantee the exact regulation of the inverter AC-side output voltage $v_{odq}$ to a desired set-point $\mathbf{e}V_n$, $V_n \in \mathbb{R}_{>0}$. As grid-forming inverters are required to set the voltage of the network they form, it is important that they have AC-side voltage regulation capability. In the sequel, we propose a passivity-based proportional-integral controller (PIC). This scheme supports the passivity property of (9) and stability when the inverter is connected to a load of the form (18).

### *5.1 Proportional-Integral Control*

We design a feedback controller that achieves at equilibrium $v_{odq}^* = \mathbf{e}V_n$. Consider the input $m_{dq}$ and its error signal $\tilde{m}_{dq} = m_{dq} - m_{dq}^*$. We now rewrite (25) with $m_{dq}$ substituted for $\tilde{m}_{dq}$, i.e., $m_{dq}^\top\tilde{i}_{dq}$ and $m_{dq}\tilde{v}_{dc}$ respectively are replaced by $(\tilde{m}_{dq} + m_{dq}^*)^\top\tilde{i}_{dq} + \tilde{m}_{dq}^\top i_{dq}^*$, and $(\tilde{m}_{dq} + m_{dq}^*)\tilde{v}_{dc} + \tilde{m}_{dq}v_{dc}^*$. We propose the proportional-integral controller (referred to as PIC) given by

$$\dot{\tilde{\eta}}_{dq} = y_{dq} \quad (28a)$$

$$\tilde{m}_{dq} = -\lambda_P y_{dq} - \lambda_I\tilde{\eta}_{dq} \quad (28b)$$

where $y_{dq} = \tilde{i}_{dq}v_{dc,ref} - i_{dq}^*\tilde{v}_{dc}$; $\lambda_P, \lambda_I \in \mathbb{R}_{>0}$ are the proportional and integral gains. We follow the approach in Arghir et al. (2018) to obtain $i_{dq}^*$, i.e. the equilibrium solution of (6), (24) with $v_{odq}^* = \mathbf{e}V_n$, $v_{dc}^* = v_{dc,ref}$ gives $i_{dq}^* = (G_s\mathbf{I}_2 - \omega^* C_f\mathcal{J})\mathbf{e}V_n + i_{odq}^*$; $m_{dq}^* = \frac{2}{v_{dc,ref}}[(R_f\mathbf{I}_2 - \omega^* L_f\mathcal{J})i_{dq}^* + \mathbf{e}V_n]$. It should be noted that in a practical implementation an integrator [2] is usually used to obtain the target $i_{dq}^*$. This is omitted here to simplify the analysis and will be studied in future work. We now state Proposition 5.1.

*Proposition 5.1.* (Proportional-Integral Control). Consider the system (25), (28). If condition (12) holds for an equilibrium point with $v_{odq}^* = \mathbf{e}V_n$, $v_{dc}^* = v_{dc,ref}$, the system with

[2] In particular, $i_{dq}^* = -\kappa_I\int(v_{odq} - \mathbf{e}V_n)\,\mathrm{d}\tau$

input $-\tilde{v}_{bdq}$ and output $\tilde{i}_{odq}$, is passive. Moreover, suppose the AC-side is connected to load (18) and condition (19) is satisfied, then the equilibrium point of the system (25), (28), (20) is globally asymptotically stable.

The proof is analogous to that of Theorem 4.8.

## 6. SIMULATION RESULTS

We implement the proposed frequency controller (9) together with the DC voltage controller (24), and PIC (28) on a two-inverter test system shown in Fig. 2 to validate their performance. A detailed and realistic inverter model which includes the on/off actuation of the electronic switches is used in the simulation. The line dynamics are also incorporated in the simulations with these simulated in their *abc* representation. The inverter parameters are $R_f = 0.05\ \Omega$, $L_f = 8$ mH, $C_f = 50\ \mu$F, $R_c = 0.03\ \Omega$, $L_c = 7$ mH, $G_{dc} = 10$ mS, $G_s = 3$ mS, $\omega_n = 2\pi(50)$ rad/s, $k_p = 0.0094$; $\Lambda_P, \lambda_P = 1; \Lambda_I, \lambda_I = 10$; $V_{dc_{ref}} = 1000$ V, $i_{dc_{ref}} = 3$ A. The line parameters are $R_{12} = 0.4\ \Omega$, $L_{12} = 6$ mH; constant impedance loads with nominal rating [3] $P_{\ell 1} = 1$ kW, $Q_{\ell 1} = 100$ Var and $P_{\ell 2} = 1$ kW, $Q_{\ell 2} = 100$ Var are connected to buses 1 and 2 respectively (Fig. 2). The simulation is performed in the presence of load variations. At $t = 0.7$ s, an RL load, $R_{\ell 1}, = 20\ \Omega$, $L_{\ell 1} = 40$ mH, is switched on at bus 1, and an equivalent load $R_{\ell 2}, = 20\ \Omega$, $L_{\ell 2} = 40$ mH is switched off at bus 2 at $t = 2.2$ s.

Fig. 3a shows that the frequency controller (9) provides steady-state accurate power sharing between the inverters directly linked to their corresponding droop gains (equal droop gains, i.e. $k_{p,1} = k_{p,2}$, are chosen). The power sharing is achieved without communication and no oscillations are observed on the power responses. Fig. 3b shows that the frequency (note $f = \omega/2\pi$) of the inverters adapts to the load step changes and the two frequencies are identical at steady state. This demonstrates the synchronisation of the inverters. Note that a steady-state frequency deviations from the nominal is expected as (9) is a primary control scheme. The restoration of the frequency to the nominal can be achieved with suitable secondary control, and will be considered in future work. It is evident in Figs. 3c, 3d that the inverter DC voltage and AC-side output voltages track their respective references 1000 V and 311 V using local measurements. The chosen value of $k_p$ allows the equilibrium points to always satisfy conditions (12) and (19) respectively, thus leading to a stable operation and good dynamic responses.

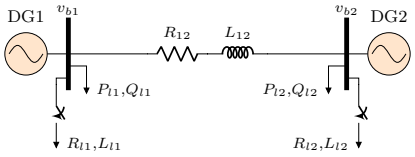


Fig. 2. Two-inverter test system.

## 7. CONCLUSION

We have proposed frequency and voltage control schemes for grid-forming inverters. In particular, we have proposed a frequency control scheme that employs the inverter output current direct coordinate as feedback to adapt the frequency so as to achieve active power sharing. Our frequency controller enforces synchronisation, guarantees accurate power sharing, and also provides appropriate passivity properties. We further designed a voltage control scheme that regulates the inverter AC-side output voltage to the desired set-point and preserves the inverter passivity properties. Numerical simulations on advanced models were also carried out which demonstrated that our controllers provide also good transient performance. Future work includes the study of these controllers in complex networks on a common reference frame, and secondary control schemes that eliminate the steady-state frequency deviation caused by primary control.

[3] Nominal power at the reference voltage provided to the inverter.

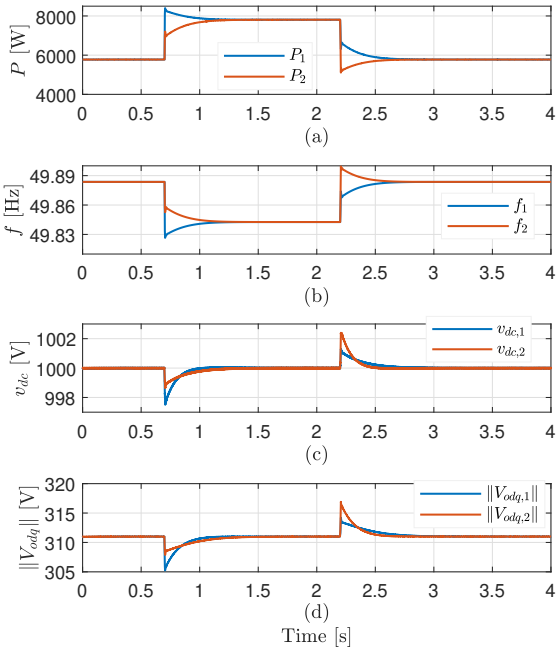


Fig. 3. System responses: (a) Active power; (b) Frequency; (c) DC voltage; (d) Inverter AC-side output voltage.

## REFERENCES


Aracil, J. and Gordillo, F. (2002). On the control of oscillations in dc-ac converters. In *IEEE 2002 28th Annual Conference of the Industrial Electronics Society. IECON 02*, volume 4, 2820–2825 vol.4.

Arghir, C., Jouini, T., and Dörfler, F. (2018). Grid-forming control for power converters based on matching of synchronous machines. *Automatica*, 95, 273 – 282.

Chandorkar, M.C., Divan, D.M., and Adapa, R. (1993). Control of parallel connected inverters in standalone ac supply systems. *IEEE Transactions on Industry Applications*, 29(1), 136–143.

Khalil, H.K. (2015). *Nonlinear control*. Pearson New York.

Milano, F., Dörfler, F., Hug, G., Hill, D.J., and Verbič, G. (2018). Foundations and challenges of low-inertia systems (invited paper). In *2018 Power Systems Computation Conference (PSCC)*, 1–25.

Ojo, Y., Watson, J., and Lestas, I. (2019). An improved control scheme for grid-forming inverters. In *2019 IEEE PES Innovative Smart Grid Technologies Europe (ISGT-Europe)*, 1–5. IEEE.

Pogaku, N., Prodanovic, M., and Green, T.C. (2007). Modeling, analysis and testing of autonomous operation of an inverter-based microgrid. *IEEE Transactions on Power Electronics*, 22(2), 613–625.

Watson, J., Ojo, Y., Spanias, C., and Lestas, I. (2019). Stability of power networks with grid-forming converters. In *2019 IEEE Milan PowerTech*, 1–6. IEEE.